

Machine learning approach for quantum non-Markovian noise classification

Stefano Martina,^{*} Stefano Gherardini,[†] and Filippo Caruso[‡]

*Dept. of Physics and Astronomy & European Laboratory for Non-Linear Spectroscopy (LENS),
University of Florence, via G. Sansone 1, 50019 Sesto Fiorentino, Italy.*

In this paper, machine learning and artificial neural network models are proposed for quantum noise classification in stochastic quantum dynamics. For this purpose, we train and then validate *support vector machine*, *multi-layer perceptron* and *recurrent neural network*, models with different complexity and accuracy, to solve supervised binary classification problems. By exploiting the quantum random walk formalism, we demonstrate the high efficacy of such tools in classifying noisy quantum dynamics using data sets collected in a single realisation of the quantum system evolution. In addition, we also show that for a successful classification one just needs to measure, in a sequence of discrete time instants, the probabilities that the analysed quantum system is in one of the allowed positions or energy configurations, without any external driving. Thus, neither measurements of quantum coherences nor sequences of control pulses are required. Since in principle the training of the machine learning models can be performed a-priori on synthetic data, our approach is expected to find direct application in a vast number of experimental schemes and also for the noise benchmarking of the already available noisy intermediate-scale quantum devices.

Noise sensing aims at discriminating, and possibly reconstructing, noise profiles that affect static parameters and dynamical variables of the evolution of classical and quantum systems [1–4]. Regarding the latter, which constitute the main object of our discussion, noise usually destroys partially the coherent evolution of the investigated (open) quantum system, interacting with an external environment or simpler with other quantum or classical systems [5, 6]. In such scenario, noise can be generally modelled as a stochastic process, distributed according to an unknown probability distribution [7, 8]. Several techniques, at both the theoretical and experimental side, have been recently developed for the inference of the unknown noise distribution and detect, if present, non-zero time-correlations among adjacent samples (over time) of the noise process [9–18]. However, most of them suffer of the need to be able to fully, or almost totally, control the quantum system, so as to generate multiple control sequences (e.g., dynamical decoupling ones [19–21]) each of them being sensitive to a different component of the noise to be inferred [22, 23]. Moreover, in reference [24] a diagnostic protocol for the detection of correlations among arbitrary sets of qubits have been lately tested on a 14-qubit superconducting quantum architecture, by discovering the persistent presence of long-range two-qubit correlations.

In this paper, we exploit for the first time powerful statistical tool, based on Machine Learning (ML) techniques [25, 26], to efficiently carry out quantum noise classification with high accuracy. The proposed methods are designed to distinguish between Independent and Identically Distributed (i.i.d.) noise sequences and noise samples originated by a non-trivial memory kernel, thus characterised by specific time-correlation parameters. It

is worth reminding that, in the latter case, the dynamics of the stochastic quantum system turns out of being non-Markovian, in the sense that samples of its state in different time instants are correlated [27, 28]. This entails that the propagation of the system in subsequent time intervals is highly influenced by its previous states, even occurring in the early stages of the dynamics. This effect corresponds to a two-fold exchange of information between the system and the external sources, and thus has also applications for quantum sensing.

To effectively present our novel approach and demonstrate its efficacy in discriminating Markovian and non-Markovian noise sources, we focus on the single-particle case and specifically on the dynamics of a single quantum walker randomly moving on a graph \mathcal{G} [29–33], as generated by a stochastic Schrödinger equation. In this context, by training a properly-designed artificial neural network model via the probabilities that the quantum walker is in each node of the graph \mathcal{G} at discrete time instants, we are going to show that it is possible to accurately discriminate between different noise sources and identify the possible presence of noise time-correlation, by observing only the single realisations of the stochastic quantum dynamics.

To perform quantum noise classification, Support Vector Machines (SVMs), Multi-Layer Perceptrons (MLPs) and Recurrent Neural Networks (RNNs) [34–37] are successfully trained on six data sets (each of them composed by 20 000 realisations) that have been properly generated to carry out binary classification of noisy quantum dynamics. Once trained, the proposed ML-models are able to reach a classification accuracy (defined by the number of correctly classified realisations over their total number) up to 97%. A pictorial representation of the proposed ML procedure is depicted in Fig. 1.

Compared to existing sensing techniques, our approach provides several advantages. First of all, the training of the artificial neural network model can be performed on synthetic data without necessarily resorting to experi-

^{*} stefano.martina@unifi.it

[†] gherardini@lens.unifi.it

[‡] filippo.caruso@unifi.it

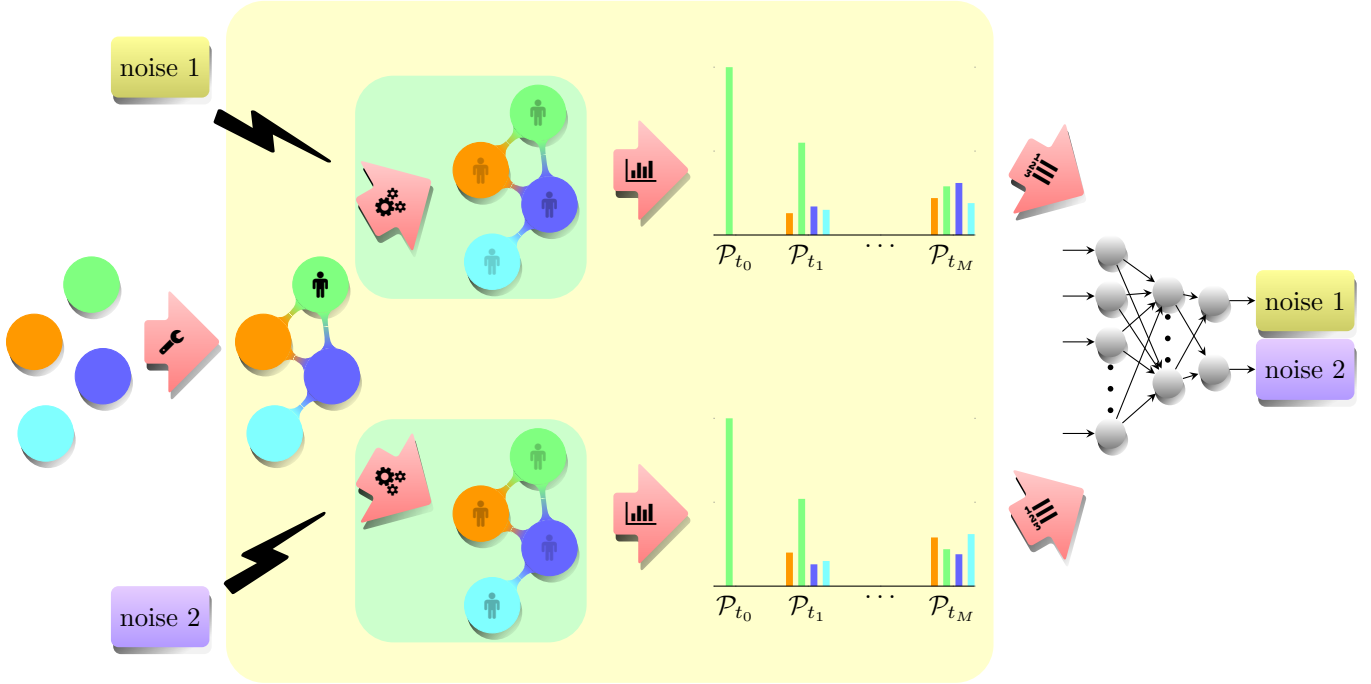


Figure 1. Pictorial representation of the proposed machine learning procedure for quantum noise classification. Specifically, for a fixed set of nodes \mathcal{N} (coloured circles) and two types of noise sources, a random topology \mathcal{E} (edges linking the coloured circles) and a random initial distribution \mathcal{P}_{t_0} of the system (black pawn) determine the evolution of the noisy quantum dynamics for M consecutive steps (small green plate). After the dynamics, all the distributions \mathcal{P}_{t_k} , in correspondence of the $M + 1$ time instants t_k with $k = 0, \dots, M$, are collected and recorded with the noise type label. Then, a data set of N different realisations (big yellow plate) is used to train a ML model (a neural network in the figure) to classify the noise sources.

mental data. Moreover, if useful, one could improve the presented approach over time, once that further information on the experimental setup, as well as experimental data, are collected. This will allow also to make the modelling more accurate by iterative optimizations in presence of artificial known noise sources. Furthermore, one single ML architecture can be designed, trained and then adopted to accurately discriminate i.i.d. and correlated noise sources. Finally, it is worth mentioning that our ML-based approach allows for non-Markovian noise classification by processing only measurements of the quantum system populations. For example, for the quantum walker case, this means that we need to record, in discrete time instants, the probabilities (sometimes called “occupation probabilities”) that the walker is in the positions (even part of them) identified by the nodes of graph \mathcal{G} . All these advantages constitute the novelty core of our paper, which is expected to find direct applications in any experimental setup affected by noise sources and even in the available or coming quantum devices where a noise certification could be crucial before performing any task.

THEORY

Stochastic quantum dynamics

According to the quantum random walk formalism (generalising classical random walks to the quantum domain), we consider a single quantum random walker that moves on a complex graph \mathcal{G} . The latter is described by the pair $(\mathcal{N}, \mathcal{E})$, where \mathcal{N} denotes the set of nodes or vertices while \mathcal{E} the set of links, denoted as $s \leftrightarrow \ell$, coupling pairs of nodes, with $s, \ell = 1, \dots, d$ and d being the total number of nodes. Each node is associated to a different walker position, while the links correspond to the possibility that the walker can jump from a node to another. In particular, the links in \mathcal{E} can be summarised in the adjacency matrix A_t (time-dependent operator in the more general case) whose elements are given by

$$A_t^{(s, \ell)} = \begin{cases} g_t & \text{if } s \leftrightarrow \ell \in \mathcal{E} \\ 0 & \text{if } s \leftrightarrow \ell \notin \mathcal{E}. \end{cases} \quad (1)$$

In this way, we are implicitly assuming that all the links are equally coupled with the same weight equal to g_t that is a time-dependent parameter.

The coupling g_t can be described as a stochastic process defined by the collection of random variables $\mathbf{g} \equiv (g_{t_0}, \dots, g_{t_{M-1}})^T$, with $(\cdot)^T$ being the transposition op-

eration, in correspondence of the discrete time instants t_k with $k = 0, \dots, M - 1$. At each t_k , g_t is sampled by a specific probability distribution $\text{Prob}(g)$ and then is assumed to remain constant at the extracted value for the entire time interval $[t_k, t_{k+1}]$. Moreover, for simplicity, also the value $\Delta \equiv t_{k+1} - t_k$ is taken constant for every $k = 0, \dots, M - 1$. Moreover, the stochastic process g_t is considered to take D different values $g^{(1)}, \dots, g^{(D)}$ with probabilities $p_{g^{(1)}}, \dots, p_{g^{(D)}}$, such that

$$\text{Prob}(g) = \sum_{j=1}^D p_{g^{(j)}} \delta(g - g^{(j)}) \quad (2)$$

is provided by a discrete probability distribution with D values, where $\delta(\cdot)$ denotes the Kronecker delta.

If \mathbf{g} is provided by a collection of i.i.d. random variables sampled from the probability distribution $\text{Prob}(g)$, then the noise sequence affecting the link strength g is uncorrelated over time. Conversely, in case the occurrence of the random value $g^{(j)}$, $j = 1, \dots, D$, at the discrete time instants t_k , $k = 0, \dots, M - 1$, depends on the sampling of g at previous time instants, the noise sequence is time-correlated and the noise is denoted as *coloured noise process*. In this regard, notice that the value of the parameters, which define the correlation among different samples of noise in single time-sequences, uniquely set the colour of the noise. In our quantum dynamical model, we adopt as correlation model the well-known formalism of time-homogeneous *discrete Markov chains* [38]. The latter can be graphically interpreted as a state-machine that assign the conditional probability of “hopping” from each possible value of g to an adjacent one at consecutive time instants. Each conditional probability at any time t is defined by a *transition matrix* T that is a left or right stochastic operator. In this regard, let us remind that discrete Markov chains differ by a parameter m named as *order*. In a Markov chain of order m , future realisations of the sampled random variable (e.g. our g_t) depend on the past m realisations in previous time instants. In this paper, we will consider $m = 1$ -order discrete Markov chains, namely correlated noise sequence characterised by a single (1-step) transition matrix T that we aim to discriminate by means of properly-developed ML techniques. Here, it is worth stressing that this choice is simply dictated by our desire to illustrate effectively our results, and not by intrinsic limitations of the methods we are going to propose. As an example, let us assume $m = 1$ and $D = 2$. In this specific case, by taking the conditional probabilities $p(g_{t_k} | g_{t_{k-1}})$ with g_{t_k} equal to $g^{(1)}$ or $g^{(2)}$ for any k , it holds that $p(g_{t_k} | g_{t_{k-1}})$ is equal to one of the elements within the following transition matrix:

$$T = \begin{pmatrix} p(g_{t_k} = g^{(1)} | g_{t_{k-1}} = g^{(1)}) & p(g_{t_k} = g^{(1)} | g_{t_{k-1}} = g^{(2)}) \\ p(g_{t_k} = g^{(2)} | g_{t_{k-1}} = g^{(1)}) & p(g_{t_k} = g^{(2)} | g_{t_{k-1}} = g^{(2)}) \end{pmatrix}. \quad (3)$$

Thus, the stochastic realisations of g in different time

instants are not correlated only if $T = \mathbb{I}_D/2$, with \mathbb{I}_D the identity matrix of size D .

Here, we are interested in discriminating features of the noise distribution $\text{Prob}(g)$ that affects the coupling strength of the graph \mathcal{G} ’s links at discrete time instants. Besides, we assume that nodes have the same energy. Without loss of generality, one is allowed to set such energy to zero, with the result that the Hamiltonian H_t (Hermitian operator) associated to the quantum walker is identically equal to the adjacency matrix A_t , i.e., $H_t = A_t$ for any time instant t . The state of the quantum walker, moving on a graph with d nodes, is provided by the well-known density operator ρ_t that is an Hermitian, positive semi-definite, idempotent operator matrix with trace 1 for any t . By using the vectorisation operation $\text{vec}[\cdot]$, ρ_t can be converted into the column vector

$$\begin{aligned} \boldsymbol{\lambda}_t &\equiv \text{vec}[\rho_t] \\ &= (\rho_t^{(11)}, \dots, \rho_t^{(d1)}, \rho_t^{(12)}, \dots, \rho_t^{(d2)}, \dots, \rho_t^{(dd)}) \in \mathbb{C}^{d^2} \end{aligned}$$

with $\rho_t^{(s,\ell)}$ denoting the $s\ell$ -element of ρ_t . The state $\boldsymbol{\lambda}_t$ is a vector of d^2 elements belonging to the space of complex numbers. Since the walker is a quantum system and can thus live in a superposition of positions whereby also quantum coherence plays an active role, d elements of $\boldsymbol{\lambda}_t$ corresponds to the probabilities of finding the walker in each of the allowed positions (such terms are denoted as *populations*), while the other elements are the so-called *quantum coherence* terms that identify interference patterns between the nodes of the graph. Thanks to the vectorisation of ρ_t , the ordinary differential equation, governing the dynamics of the quantum walker, is recast in a linear differential equation for $\boldsymbol{\lambda}_t$, i.e.,

$$\begin{aligned} \frac{\partial}{\partial t} \boldsymbol{\lambda}_t &= \mathcal{L}_t \boldsymbol{\lambda}_t \\ \mathcal{L}_t &\equiv -\frac{i}{\hbar} (\mathbb{I}_d \otimes A_t - A_t^T \otimes \mathbb{I}_d) \end{aligned}$$

with \otimes Kronecker product. By construction, \mathcal{L}_t is a skew-Hermitian operator for any time instant t , i.e. $\mathcal{L}_t^\dagger + \mathcal{L}_t = 0 \ \forall t$.

Problem formulation

Our aim is to identify the presence of noise sources on the coupling g_t of the adjacency matrix A_t , and then discriminate among different noise probability distributions $\text{Prob}(g)$ and correlation parameters in the samples of the time-sequences \mathbf{g} , by only measuring the walker populations at the discrete time instants t_k in a single run of the quantum system dynamics. We collect such populations in the vectors $\mathcal{P}_{t_k} \in \mathbb{R}^d$ that have as many elements as the nodes of the graph. After each stochastic evolution of the quantum walker, \mathcal{P}_{t_k} takes different values depending on the specific realisation of \mathbf{g} .

Data set

In the generation of the data (to be used to train the ML-models), we consider two variants of three different classification problems. In doing this, we set $M = 15$ as the number of evaluations (measurements) of the quantum walker dynamics, $d = 40$ the number of nodes of the graph \mathcal{G} and the total dynamical times respectively to $t_M = 1$ and $t_M = 0.1$, each of them corresponding to a specific variant. For each one of the two settings, we generate three different balanced data sets of $2N = 20\,000$ samples, by taking random topologies (i.e., random configurations for the set \mathcal{E} of links) and random initial states for the walker dynamics. The first data set, which we call **IID**, is suitable for a supervised binary classification task that discriminates between two different i.i.d. noisy quantum dynamics, where the noise sources have the same support but different probability distribution $\text{Prob}(g)$. The second one, named here as **NM**, concerns the classification of two different coloured noisy quantum dynamics with noise sources again having the same support but different $\text{Prob}(g)$ (the same ones as in **IID**) and a transition matrix T . Finally, the third one, called **VS**, is the data set created for the classification between stochastic quantum dynamics affected respectively by an i.i.d. and a coloured noise with same support and $\text{Prob}(g)$. Note that choosing graphs with random links allows to increase the statistical variability of the input data, such that the ML algorithms can learn to classify noise sources independently of the graph topology. The aim is to prevent that the ML-models rely only on features specific to a small class of topologies.

Table I. Example of a part of \mathcal{P}_{t_k} for all the discrete time instants t_k for a noisy quantum dynamics with i.i.d. noise sources and $t_{15} = 0.1$. In the Table, $\mathcal{P}_{t_k}^{(s)}$ denotes the s -th element of the vector \mathcal{P}_{t_k} for any t_k , $k = 0, \dots, 15$.

	$\mathcal{P}_{t_k}^{(35)}$	$\mathcal{P}_{t_k}^{(36)}$	$\mathcal{P}_{t_k}^{(37)}$	$\mathcal{P}_{t_k}^{(38)}$	$\mathcal{P}_{t_k}^{(39)}$	$\mathcal{P}_{t_k}^{(40)}$
t_0	0.00	0.00	0.00	0.00	1.00	0.00
t_1	0.00	0.00	0.00	0.00	0.99	0.00
t_2	0.00	0.00	0.00	0.00	0.93	0.00
t_3	0.00	0.00	0.01	0.01	0.85	0.01
t_4	0.00	0.01	0.01	0.01	0.78	0.01
t_5	0.01	0.01	0.01	0.01	0.69	0.01
t_6	0.01	0.02	0.01	0.01	0.63	0.00
t_7	0.01	0.02	0.01	0.01	0.57	0.00
t_8	0.01	0.02	0.01	0.01	0.52	0.00
t_9	0.02	0.02	0.01	0.01	0.45	0.00
t_{10}	0.02	0.02	0.02	0.02	0.37	0.01
t_{11}	0.01	0.02	0.02	0.03	0.29	0.01
t_{12}	0.01	0.01	0.03	0.04	0.20	0.02
t_{13}	0.01	0.01	0.04	0.04	0.14	0.01
t_{14}	0.01	0.02	0.04	0.05	0.08	0.01
t_{15}	0.01	0.02	0.04	0.05	0.06	0.01

Table II. Example of a part of \mathcal{P}_{t_k} for all the discrete time instants t_k for a noisy quantum dynamics with i.i.d. noise sources and $t_{15} = 1$. Again, $\mathcal{P}_{t_k}^{(s)}$ denotes the s -th element of the vector \mathcal{P}_{t_k} for any t_k , $k = 0, \dots, 15$. The topology and the initial state, for this example, are the same of those in Table I.

	$\mathcal{P}_{t_k}^{(35)}$	$\mathcal{P}_{t_k}^{(36)}$	$\mathcal{P}_{t_k}^{(37)}$	$\mathcal{P}_{t_k}^{(38)}$	$\mathcal{P}_{t_k}^{(39)}$	$\mathcal{P}_{t_k}^{(40)}$
t_0	0.00	0.00	0.00	0.00	1.00	0.00
t_1	0.02	0.02	0.01	0.01	0.45	0.00
t_2	0.01	0.01	0.02	0.03	0.05	0.02
t_3	0.00	0.00	0.00	0.00	0.13	0.02
t_4	0.02	0.01	0.01	0.01	0.12	0.02
t_5	0.01	0.01	0.03	0.03	0.06	0.01
t_6	0.01	0.01	0.01	0.01	0.01	0.00
t_7	0.04	0.03	0.01	0.06	0.11	0.00
t_8	0.04	0.00	0.03	0.11	0.11	0.03
t_9	0.03	0.00	0.03	0.01	0.01	0.10
t_{10}	0.05	0.01	0.01	0.04	0.08	0.04
t_{11}	0.01	0.03	0.02	0.00	0.08	0.02
t_{12}	0.00	0.05	0.02	0.04	0.00	0.06
t_{13}	0.01	0.03	0.00	0.02	0.05	0.07
t_{14}	0.00	0.00	0.00	0.01	0.12	0.00
t_{15}	0.00	0.00	0.01	0.04	0.10	0.01

As it will be explained in the following, some ML-models that we are going to introduce will use only the last distribution $\mathcal{P}_{t_{15}}$ as input, while other ML-models will take all the \mathcal{P}_{t_k} for any t_k . Each data set is balanced split in a *training set* of 12 000 samples, a *validation set* of 4 000 samples, and a *test set* of 4 000 samples.

Let us point out that in the Tables I and II we have deliberately chosen to plot the occupation probabilities \mathcal{P}_{t_k} just for the **IID** case, because we are here interested in looking for the difference between choosing $t_{15} = 0.1$ or 1. The latter identify the two different variants of the generated data set: The duration $t_{15} = 0.1$ of the quantum system dynamics, as in the example in Table I, is the minimal one to observe the diffusion of the system population outside the node on which has been initialised. However, as it will be verified by our experiments and explained later, with this choice one has that, by taking $t_{15} = 0.1$, the classification problem results quite straightforward. Indeed, just basic ML-models that only read $\mathcal{P}_{t_{15}}$ (thus, only the final distribution \mathcal{P}) are able to correctly classify between two noisy quantum dynamics. Therefore, it was more interesting to increase the value of t_{15} up to $t_{15} = 1$. It (as in the example of Table II) leads to more complex data sets, and only deep learning models that read all the \mathcal{P}_{t_k} are able to classify noisy quantum dynamics. It is also worth noting that, according to preliminary simulations, with a value of $t_{15} \gg 1$ our trained ML-models do not reach more than 60% of accuracy for the test set.

Machine Learning models

Here, we compare classic machine learning algorithms, as SVM, with more recent deep learning approaches to perform binary supervised classification tasks on the simulated data. With \mathcal{P}_{t_k} as input, we are able to classify between: (i) two different probability distributions $\text{Prob}(g)$ associated to i.i.d. noise sources; (ii) two different $\text{Prob}(g)$ for coloured noise processes; and (iii) an i.i.d. and a coloured noise with the same support g and distribution $\text{Prob}(g)$.

Support Vector Machine

SVM is a generalisation of the Support Vector Classifier (SVC) that, in turn, is an improved version of the Maximal Margin Classifier (MMC) [26]. A generic binary data set in input to these ML-models is usually represented by a set of n points $\mathbf{x}_q \in \mathbb{R}^p$, with $q = 1, \dots, n$, each of them living in the p -dimension space of the features. A feature is a distinctive attribute of each element of the data set. Each point \mathbf{x}_q is associated to one of two different classes with binary labels ± 1 , depending on the specific classification problem that we are solving. Thus, after this classification, the points are provided by the scalars $y_q \in \{-1, 1\}$, with $q = 1, \dots, n$.

MMCs aim at finding the hyperplane separating the two aforementioned classes of points, such that the distance between the hyperplane and the nearest points of the classes (commonly denoted as *margin*) is maximised. If the points of the data set are not linearly separable, then the value of the margin is negative. In such a case, the MMCs cannot be adopted. SVCs increase the performance of MMCs, by allowing some points of the data set, called *slack variables*, to be in the opposite part of the hyperplane with respect to the others of the belonging class. If the data set exhibits a non-linear bound between the two classes of points, SVCs are not able to correctly separate them, albeit the method returns a solution. Finally, SVMs extend the capabilities of SVCs by increasing the number of dimensions of the feature-space, such that in the new space the data set becomes linearly separable.

Multi-Layer Perceptron

There are several classification problems (as for example the ImageNet Large Scale Visual Recognition Challenge [39] employing millions of images with hundreds of categories) that are solved through SVM but without a low enough residual classification error. For this reason, to improve the performance in solving classification problems, Artificial Neural Networks (ANNs) have recently been (re-)introduced as more-performing tools, and since 2012 have been extensively used [36, 39–41]. The basic model of the ANNs is the MLP. The latter is composed

of a variable number of fully connected layers, each of them with a variable number of artificial neurons. A single artificial neuron with I inputs (\mathbf{x}) calculates the output as

$$\hat{y} \equiv \sigma(\mathbf{w}^T \cdot \mathbf{x} + b)$$

that is the weighted sum of the inputs $\mathbf{x} \in \mathbb{R}^I$ with weights $\mathbf{w} \in \mathbb{R}^I$, plus a bias term $b \in \mathbb{R}$, followed by a nonlinear activation function $\sigma : \mathbb{R} \rightarrow \mathbb{R}$. The most common activation functions $\sigma(\cdot)$ are: The *sigmoid* $\sigma(x) \equiv (1 + e^{-x})^{-1}$; the *hyperbolic tangent* $\sigma(x) \equiv \tanh(x)$; and the *rectifier* $\sigma(x) \equiv \max(0, x)$ [42, 43]. A single MLP-layer, composed of O neurons with I inputs, calculates

$$\hat{\mathbf{y}} \equiv \sigma(W^T \cdot \mathbf{x} + \mathbf{b}) ,$$

where $\hat{\mathbf{y}} \in \mathbb{R}^O$ is the output vector, $W \in \mathbb{R}^{I \times O}$ is a matrix that collects all the weight vectors of the single neurons, and $\mathbf{b} \in \mathbb{R}^O$ is the vector of the biases. Finally, an MLP with L layers calculates

$$\mathbf{h}[l] \equiv \sigma(W[l]^T \cdot \mathbf{h}[l-1] + \mathbf{b}[l]) \quad (4)$$

with $l = 1, \dots, L$ (index over the layers) and $\mathbf{h}[0] \equiv \mathbf{x}$. Thus, $\hat{\mathbf{y}} \equiv \mathbf{h}[L]$ is the output of the MLP, where $W[l]$ and $\mathbf{b}[l]$ are, respectively, the weights and the biases of the l -th layer. Also the activation function may change depending on the specific layer. More concisely, the MLP can be denoted by the function

$$\hat{\mathbf{y}} = f(\mathbf{x}; \theta, \xi) \quad (5)$$

of the inputs \mathbf{x} . The function f is parametrised by the set $\theta \equiv \{W[1], \mathbf{b}[1], \dots, W[L], \mathbf{b}[L]\}$ and by the fixed hyperparameters ξ defining the number, the dimension, and the activation functions of the MLP layers.

Supervised Training

Let us now introduce the supervised learning process. For the sake of clarity, we just refer to the training of the MLP; however, the same notions can be applied in general to the supervised learning of vast majority of ANNs.

Eq. (5) behaves like a generic function approximator [44]. Ideally, in the training process we would like to find the parameters

$$\theta^* = \arg \min_{\theta} L_{\mathcal{D}}(\theta, \xi) \quad (6)$$

that minimise the theoretical risk function

$$L_{\mathcal{D}}(\theta, \xi) \equiv \mathbb{E}_{(\mathbf{x}, \mathbf{y}) \sim \mathcal{D}} [\ell(f(\mathbf{x}; \theta, \xi), \mathbf{y})] , \quad (7)$$

i.e., the expected value of ℓ for (\mathbf{x}, \mathbf{y}) sampled from the distribution \mathcal{D} that generates the data set. In Eq. (7), $\ell : \mathbb{R}^{O \times O} \rightarrow \mathbb{R}^+$ denotes the loss function (usually taken as a differentiable function, apart removable discontinuities) that measures the distance between the prediction

$\hat{\mathbf{y}}$ and the desired output \mathbf{y} . In general, the distribution \mathcal{D} is unknown; thus, the minimisation problem in Eq. (6) cannot be neither calculated nor solved. Indeed, one can dispose of a finite set $S = \{(\mathbf{x}, \mathbf{y})_1, \dots, (\mathbf{x}, \mathbf{y})_n\}$ of samples, to train, validate and test the ML-model. By considering the partition $\{S_{tr}, S_{va}, S_{te}\}$ of S , the theoretical risk function is approximated by the empirical risk function

$$L_{S_{tr}}(\theta, \xi) = \frac{1}{|S_{tr}|} \sum_{(\mathbf{x}, \mathbf{y}) \in S_{tr}} \ell(f(\mathbf{x}; \theta, \xi), \mathbf{y}) \quad (8)$$

that is the arithmetic mean of the loss function ℓ evaluated on all the samples of the training set S_{tr} . By minimising the empirical risk function $L_{S_{tr}}(\theta, \xi)$ with respect to θ , the MLP is trained and θ^* obtained. Then, the validation set S_{va} is used to compute the empirical risk $L_{S_{va}}(\theta^*, \xi)$ that takes as input the optimal parameters attained by the minimisation of $L_{S_{tr}}$ (training stage). This procedure allows to check if the ML-model works also for unseen data. Notice that the minimisation of the training risk function $L_{S_{tr}}(\theta, \xi)$ with respect to θ is performed step-by-step over time. After each step (also called *epoch*), the validation risk $L_{S_{va}}(\theta^*, \xi)$ is evaluated, and the minimisation procedure is stopped when the time-derivative of $L_{S_{va}}(\theta^*, \xi)$ becomes positive for several epochs, thus showing *overfitting* [45]. In case such time-derivative remains negative or constant over time, the procedure is ended after a predefined number of epochs. The validation set S_{va} can be also used to explore other configurations ξ of the ML-model: this process is called *hyperparameter optimization*. In particular, after completing the training procedure using two different set of hyperparameters ξ and ξ' , we obtain two minima θ^* and θ'^* , and then compare $L_{S_{va}}(\theta^*, \xi)$ with $L_{S_{va}}(\theta'^*, \xi')$ to also choose the best hyperparameter. Finally, we use the test set S_{te} to calculate a significant metric (in our case, the classification accuracy) and report the results.

Regarding the hyperparameters optimization, it can be performed in different ways. The most basic technique is called *grid search* whereby the training and validation are carried out on a specific set of hyperparameters configurations. The *random grid search* considers configurations where each hyperparameter is randomly chosen within an a-priori fixed range of values. It has been proved to be more efficient than standard grid search [46]. A more sophisticated class of optimization methods is the *Bayesian optimization* [47] that updates, after the training of each single hyperparameters configuration, a Bayesian model of the validation error. The best hyperparameter configuration is thus chosen as the one allowing for the lower guess validation error.

Minimisation algorithms

The most used optimisation algorithm to minimise Eq. (8) is the Stochastic Gradient Descent (SGD) [48, 49]

and its adaptive variants, such as Adaptive Moment Estimation (ADAM) [50], that changes the value of the learning rate η (i.e., the descent step) at each iteration. After having calculated the predictions $\hat{\mathbf{y}}$, the loss function $\ell(\hat{\mathbf{y}}, \mathbf{y})$ is propagated backwards (*backpropagation*) in the ANN and its gradient in the weight space is calculated. Overall, the optimisation process consists in iteratively updating the value of the weights θ according to the relation

$$\theta_i = \theta_{i-1} - \eta \nabla_{\theta} L_{S_b}(\theta_{i-1}, \xi),$$

where i is the index for the descent step and $S_b \subset S_{tr}$ denotes the b -th set of samples, taken from the training set and used for the computation of the gradient. If $S_b \equiv S_{tr}$, the algorithm is called *batch* SGD; if S_b contains only one element is called *on-line* SGD; finally, the most common approach (we use it here) is *mini-batch* SGD that consider $|S_b| = B$ with B a fixed dimension. Hence, the update of θ follows the descent direction of the gradient, with a magnitude determined by the learning rate η .

Now, let us introduce the specific loss function ℓ considered in this paper. For classification problems with two or more classes, a common choice for ℓ is the *categorical cross entropy*, which is defined as

$$\ell(\hat{\mathbf{y}}, \mathbf{y}) = - \sum_{j=1}^O y^{(j)} \log \hat{y}^{(j)}. \quad (9)$$

This function measures the dissimilarity between two or more probability distributions. Thus, to properly use the categorical cross entropy, it is convenient to choose the desired outputs \mathbf{y} as Kronecker delta functions centered around the indices associated to each class to be classified. The model output $\hat{\mathbf{y}}$, instead, is normalised so that it represents a discrete probability distribution, i.e., a vector of positive elements summing to 1. This operation is obtained by using *softmax* [35] as the activation function of the last layer:

$$\sigma^{(i)}(\mathbf{z}) \equiv \frac{e^{z^{(i)}}}{\sum_{j=1}^O e^{z^{(j)}}} \quad (10)$$

where $\sigma(\mathbf{z})$ is the vector having as elements $\sigma^{(i)}(\mathbf{z})$, with $i = 1 \dots, O$, and \mathbf{z} denotes the output of the last layer before the activation function.

In the experiments, the activation functions for the hidden layers of the MLP have been chosen among the sigmoid, hyperbolic tangent and rectifier functions accordingly to the hyperparameter optimization.

Recurrent Neural Networks

A RNN is an ANN specialised for sequence processing when the data set is in the form

$$S = \{(\{\mathbf{x}_1, \dots, \mathbf{x}_{\tau_1}\}, \mathbf{y})_1, \dots, (\{\mathbf{x}_1, \dots, \mathbf{x}_{\tau_n}\}, \mathbf{y})_n\}, \quad (11)$$

where τ_r defines the number of elements of the r -th sequence. RNNs can be used in tasks regarding Natural Language Processing (NLP) [37, 51–53], time series analysis [54] and, in general, all the tasks involving sequences [55]. Notice that, in general, for *sequence-to-sequence* problems also \mathbf{y} can be a sequence of elements, as for example in machine translation where the inputs and outputs of the RNN are sentences in different languages [56]. In this paper, sequence-to-sequence problems are not considered, and we take $\tau_1 \equiv \dots \equiv \tau_n \equiv \tau$.

Then, the RNN is defined by the *recurrent* relation

$$\mathbf{h}_t = r(\mathbf{x}_t, \mathbf{h}_{t-1}; \theta_r, \xi) \quad (12)$$

where $t \in \{1, \dots, \tau\}$, $\mathbf{h}_t \in \mathbb{R}^d$ is a d -dimensional vector with d being an hyperparameter belonging to ξ and $\mathbf{h}_0 = \mathbf{0}$ (vector of zeros). The recurrent relation (12) defines τ hidden representations \mathbf{h}_t (to be seen as a *memory*) of the input sequence $\{\mathbf{x}_1, \dots, \mathbf{x}_\tau\}_q$ with $q = 1, \dots, n$. If the function r is implemented as an MLP (5) that takes as input the concatenation $\mathbf{x}_t \oplus \mathbf{h}_{t-1}$ (usually called “vanilla RNN”), the model suffers the so-called *vanishing gradient problem* [57, 58] such that the weights of the last layers of the RNN are updated only with respect to the more recent input data. The vanishing gradient problem occurs when the backpropagation is performed on a high number of layers, as it could happen in our case with a large value of τ (thus meaning long input sequences). In this regard, to mitigate the vanishing gradient problem, Long Short Term Memory (LSTM) [59] and Gated Recurrent Unit (GRU) [60] have been introduced. These methods use learned gated mechanisms, based on current input data and previous hidden representations, to control how to update the current hidden representation \mathbf{h}_t . Specifically, if LSTM is used, Eq. (12) needs to be slightly modified as

$$\mathbf{s}_t = v(\mathbf{x}_t, \mathbf{s}_{t-1}; \theta_v, \xi) \quad (13)$$

$$\mathbf{h}_t = r(\mathbf{x}_t, \mathbf{s}_t, \mathbf{h}_{t-1}; \theta_r, \xi) \quad (14)$$

where $\mathbf{s}_0 = \mathbf{0}$ and v, r are, as usual, nonlinear functions. Both for GRU and LSTM, the nonlinearity of the recurrent relations is due to the adoption of the hyperbolic tangent and sigmoid functions, where the latter are employed only for the gating mechanism. It is worth noting that in Eq. (13) \mathbf{s}_t is a state vector that allows to differently propagate over time specific elements of the hidden representations \mathbf{h}_t depending on the input data. This means that, at any time t , the hidden representation \mathbf{h}_t depends not only on the input \mathbf{x}_t and the previous hidden representation \mathbf{h}_{t-1} but also on the state vector \mathbf{s}_t . For further details, refer to Refs. [37, 59, 60].

Moreover, RNNs can be extended considering more layers and processing the data bidirectionally. Regarding the latter, one can define two sets of hidden representations: One for the forward and the other for the backward direction, where the t -th hidden representation depends respectively on the $(t-1)$ -th or $(t+1)$ -th one. More

formally,

$$\mathbf{h}_t[l] = r(\mathbf{h}_t[l-1], \mathbf{h}_{t-1}[l]; \theta_r[l], \xi) \quad (15)$$

$$\tilde{\mathbf{h}}_t[l] = r(\tilde{\mathbf{h}}_t[l-1], \tilde{\mathbf{h}}_{t+1}[l]; \theta_{\tilde{r}}[l], \xi) \quad (16)$$

with $l = 1, \dots, L$ and $\mathbf{h}_t[0] \equiv \tilde{\mathbf{h}}_t[0] \equiv \mathbf{x}_t$.

Now, let us explain how to use the hidden representations to calculate the prediction $\hat{\mathbf{y}}$ in output from the ML-model. The common approach to calculate the prediction in classification problems is to use the RNN as an encoder of the sequence and to scale the dimension of the last hidden representation $\mathbf{h}_\tau[L] \oplus \tilde{\mathbf{h}}_1[L]$ (in the more general case of bidirectional models) to the one of the output vector. This scaling can be done through a fully connected layer, or, more in general, by means of an MLP, i.e.,

$$\mathbf{a} \equiv \mathbf{h}_\tau[L] \oplus \tilde{\mathbf{h}}_1[L] \quad (17)$$

$$\hat{\mathbf{y}} = f(\mathbf{a}; \theta_f, \xi). \quad (18)$$

Then, we can use SGD to minimise an empirical risk function similar to Eq. (8) of MLPs.

It is possible to consider different forms of aggregation \mathbf{a} for the hidden representations $\mathbf{h}_t[L]$, with $t = 1, \dots, \tau$, instead of using only the last hidden representation as in Eq. (17). In this regard, *attention mechanisms* [61–63], also in hierarchical forms [64], perform a weighted average of the $\mathbf{h}_t[L]$ where the weights are learned together with the ML-model. In detail, Eq. (17) becomes:

$$\mathbf{u}_t = \mathbf{h}_t[L] \oplus \tilde{\mathbf{h}}_t[L] \quad (19)$$

$$\mathbf{v}_t = \tanh(\mathbf{W}^T \cdot \mathbf{u}_t + \mathbf{b}) \quad (20)$$

$$\alpha_t \equiv \frac{e^{\langle \mathbf{v}_t, \mathbf{c} \rangle}}{\sum_{j=1}^{\tau} e^{\langle \mathbf{v}_j, \mathbf{c} \rangle}} \quad (21)$$

$$\mathbf{a} \equiv \sum_{t=1}^{\tau} \alpha_t \mathbf{u}_t, \quad (22)$$

where $\langle \cdot, \cdot \rangle$ denotes the dot product and \mathbf{c} is a learned vector that is randomly initialised and jointly learned during the training process as in Refs. [61–64]. Another form of aggregation \mathbf{a} is the *max pooling aggregation*, whereby each element $\mathbf{a}^{(j)}$ of \mathbf{a} just refers to a single value of t . In this case, Eq. (17) equals to

$$\mathbf{a}^{(j)} = \max_t \mathbf{u}_t^{(j)}. \quad (23)$$

where the expression of \mathbf{u}_t is provided by Eq. (19). In this way, each element $\mathbf{u}_t^{(j)}$ of the hidden representations (for $t = 1, \dots, \tau$) learns to detect specific features of the input data within all the interval $[1, \tau]$. This approach has been adopted in NLP tasks, and, under certain conditions, has given interpretability to the adopted RNN models [51, 52].

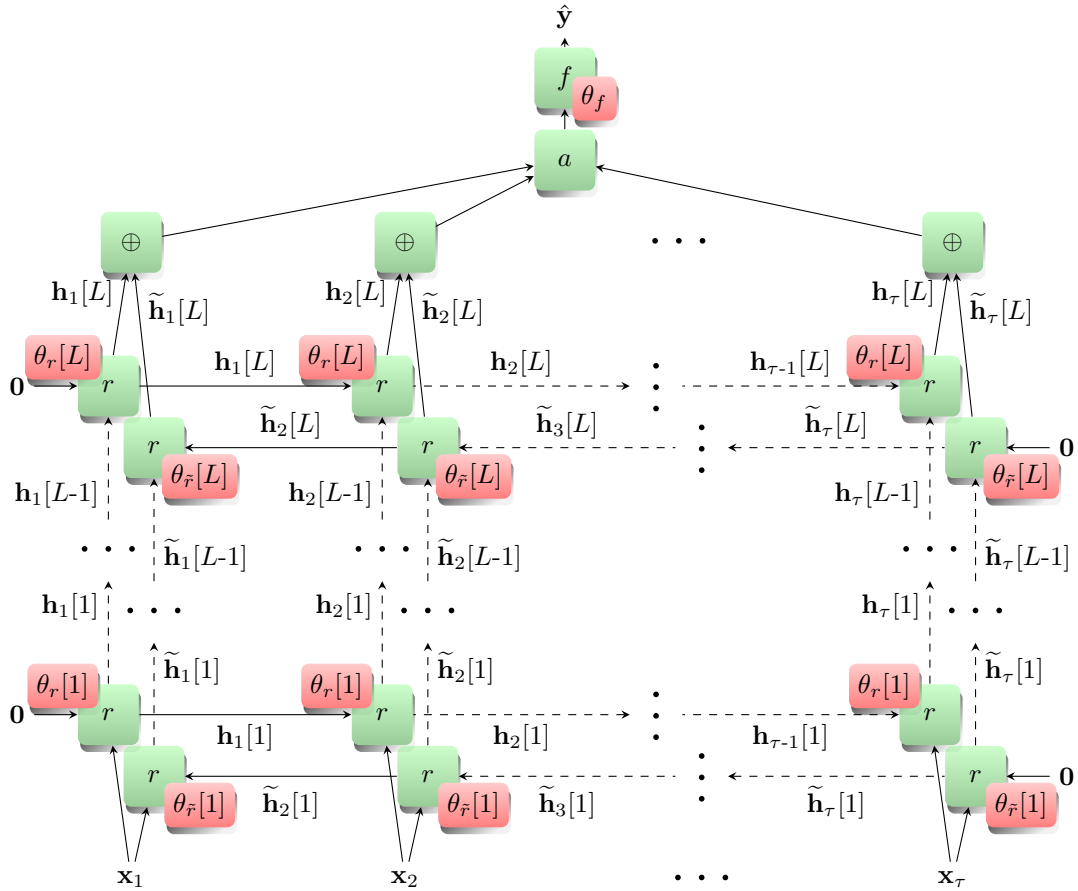


Figure 2. Diagram of a bidirectional multi-layer RNN where the nonlinear function r is defined in Eqs. (15) and (16), a can be defined either with Eq. (22) or Eq. (23), f is provided by Eq. (18), and \oplus denotes concatenation. The input sequence \mathbf{x}_t , with $t = 1, \dots, \tau$, is processed sequentially in both directions by the function r that is parametrised by the shared sets of weights $\theta_r[1]$ and $\theta_{\bar{r}}[1]$ for the forward and backward directions, respectively. The hidden representations $\mathbf{h}_1[1]$ and $\bar{\mathbf{h}}_1[1]$, in turn, are processed by the subsequent layers, parametrised by a different sets of weights, so as to obtain the final hidden representations $\mathbf{h}_t[L]$ and $\bar{\mathbf{h}}_t[L]$. Finally, a performs the aggregation of the last hidden representations adopting the attention mechanism (22) or the max pooling in Eq. (23). The classification is performed by the function f that is parametrised by θ_f . The simpler form of aggregation in Eq. (17) is not depicted in the figure.

Finally, another approach, which we do not use here, is to consider the RNN as a transducer that produces an output sequence $\hat{\mathbf{y}}_t$ for $t = 1, \dots, \tilde{\tau}$ (generally $\tilde{\tau} \neq \tau$) in correspondence of the input sequence \mathbf{x}_t with $t = 1, \dots, \tau$ [37, 56, 65].

RNNs are usually considered deep-learning models due to the high number of employed layers. The key aspect of deep learning is the automatic extraction of features by means of the composition of a large number of layers; an increasing (deep) number of layers is typically used to extract features with increasing complexity [66].

RESULTS

In our work, we consider two SVM models as baseline. The first one is denoted as **m-SVM-single** and uses as input only the final probability distribution $\mathcal{P}_{t_{15}}$ (the pre-

fix m - stands for ‘‘model’’, to avoid confusion with the algorithm name; the suffix *-single* means that it is based only on \mathcal{P}_{t_k}). Instead, the second one, which we call as **m-SVM**, uses the set of all the \mathcal{P}_{t_k} with $k = 0, \dots, 15$. For both of them, we try the following *kernels* to increase the dimension of the feature-space making linearly separable the data-set: linear, polynomial with degree 2, 3 and 4, and Radial Basis Function (RBF).

Then, we denote with **m-MLP-single** an MLP in the form of Eq. (5) with $\mathbf{x} \equiv \mathcal{P}_{t_{15}}$, and $\mathbf{y} \equiv (0, 1)$ or $(1, 0)$ to identify the two noisy quantum dynamics that we aim to classify. Differently, **m-MLP** takes as input the set of all \mathcal{P}_{t_k} .

Moreover, **m-GRU** and **m-LSTM** are unidirectional RNNs that employ the final hidden representation, which are provided by Eqs. (17) and (18). They are implemented, respectively, by exploiting the GRU and LSTM methods. In **m-GRU** and **m-LSTM**, the function f

in Eq. (18) is realised by a single-layer MLP, while $\mathbf{x}_{i+1} \equiv \mathcal{P}_{t_i}$ with $i = 0, \dots, 15$, and $\mathbf{y} \equiv (0, 1)$ or $(1, 0)$ as before. Besides, **m-biGRU** and **m-biLSTM** are the bidirectional versions of **m-GRU** and **m-LSTM**, while **m-biGRU-att** and **m-biGRU-max** are as **m-biGRU** but in addition, respectively, with the attention mechanism in Eq. (22) and the max pooling of Eq. (23) as forms of aggregation. Similarly, **m-biLSTM-att** and **m-biLSTM-max** are, respectively, the attentive and max pooling equivalents of **m-biLSTM**.

Table III. Percent accuracy γ (calculated on the test set) of the ML-models trained in the tasks of binary classification of noisy quantum dynamics with: (i) Two different i.i.d. noise sources (**IID**); (ii) two different coloured noise processes (**NM**) leading to non-Markovian dynamics; and (iii) one i.i.d. vs one coloured noise sources (**VS**). In the first three columns of the table, the total duration of the dynamics is equal to $t_{15} = 0.1$, while in the last three is $t_{15} = 1$. The first two rows of the table report the results of the ML-models that use as input only $\mathcal{P}_{t_{15}}$, while the models of the other rows take as input all the probability distributions \mathcal{P}_{t_k} for $k = 0, \dots, 15$. The highest values of the accuracy have been underlined.

		$t_{15} = 0.1$			$t_{15} = 1$			
		IID	NM	VS	IID	NM	VS	
$\mathcal{P}_{t_{15}}$	m-SVM-single	97.0	82.3	96.5	50.3	51.2	49.5	
	m-MLP-single	96.9	80.7	96.6	49.5	50.7	50.2	
		m-SVM	96.4	80.1	96.3	73.6	61.9	75.0
		m-MLP	96.7	80.7	96.3	74.0	61.4	70.7
		m-GRU	96.5	91.5	96.7	90.5	73.3	88.2
		m-LSTM	96.8	90.4	96.4	88.6	70.3	86.3
$\mathcal{P}_{t_0}, \dots, \mathcal{P}_{t_{15}}$	m-biGRU	96.6	92.2	96.6	91.0	74.6	90.6	
	m-biLSTM	96.7	89.7	96.5	90.8	70.6	87.2	
$\mathcal{P}_{t_{15}}$	m-biGRU-att	97.0	91.6	96.1	90.9	73.4	87.9	
	m-biLSTM-att	96.9	87.9	96.3	89.0	71.6	87.4	
		m-biGRU-max	96.6	92.6	96.6	91.8	76.1	90.4
		m-biLSTM-max	96.6	91.4	96.3	91.4	74.9	89.0

In Table III, for each model we report the best accuracy that is computed on the predictions performed over the test set. More formally, we define the prediction set

$$\Gamma = \{(\mathbf{y}_1, \hat{\mathbf{y}}_1), \dots, (\mathbf{y}_n, \hat{\mathbf{y}}_n)\}$$

where $\mathbf{y}_1, \dots, \mathbf{y}_n$, taken from the data set, denote the true noise sources affecting the quantum system dynamics, and $\hat{\mathbf{y}}_1, \dots, \hat{\mathbf{y}}_n$ the corresponding predictions of the ML-model. Hence, the (percent) accuracy γ , function of Γ , is provided by

$$\gamma(\Gamma) \equiv \frac{100}{n} \sum_{i=1}^n \mathbb{1} \left\{ \arg \max_{j=1,2} \hat{\mathbf{y}}_i^{(j)} = \arg \max_{j=1,2} \mathbf{y}_i^{(j)} \right\}, \quad (24)$$

where $\mathbb{1}$ is the *indicator function*

$$\mathbb{1}\{c\} \equiv \begin{cases} 1, & \text{if } c \text{ is true,} \\ 0, & \text{otherwise.} \end{cases} \quad (25)$$

DISCUSSION

In this paper, we have formulated and solved quantum non-Markovian noise classification problems by means of several machine learning techniques. In particular, the use of RNN, developed for sequence processing, was motivated by our need to deal with time-ordered sequences of data.

The correctness of our results is quantified by the values of the accuracy γ for each tested ML-models that are summarised in Table III. From the table, one can first observe that, by dealing with a total duration of the dynamics equal to $t_{15} = 0.1$, we can reach the 97% and 96.5% of accuracy for the classification tasks **IID** and **VS** via an SVM, which uses as input only the distribution $\mathcal{P}_{t_{15}}$. Instead, the task **NM** is more difficult; 82.3% of accuracy is achieved by SVM just applied on $\mathcal{P}_{t_{15}}$. MLP does not provide better results. In this case (**NM** tasks), to obtain an accuracy over 90%, one can resort to RNNs taking as inputs all the \mathcal{P}_{t_k} for $k = 0, \dots, 15$. Conversely, for a longer dynamics, i.e. with $t_{15} = 1$, we notice that using only $\mathcal{P}_{t_{15}}$ all the three classification tasks are not solved neither with SVM nor MLP. Indeed, the accuracy γ is always around 50% and the models basically perform random guesses. The accuracy is increased by means of an SVM or an MLP based on all \mathcal{P}_{t_k} , with $k = 0, \dots, 15$ as input. However, to get over 90% of accuracy on the tasks **IID** and **VS**, we need to employ RNNs. The task **NM** with $t_{15} = 1$ is the most difficult among the analysed ones, and just 76.1% of accuracy is observed using RNNs. It is worth noticing that, for the tasks with $t_{15} = 1$, we have empirically observed that the models adopting GRU perform better with respect to the ones that employ LSTM. Moreover, in the RNNs the bidirectionality allows slight improved accuracy, as well as the use of max pooling in aggregation. Conversely, the attention mechanism does not seem to be beneficial for those tasks. In the following paragraph, we will show how the classification accuracy γ is related to other important parameters for the data set generation, as the number M of the discrete time instants t_k and the interval Δ between two consecutive transitions for \mathbf{g} .

In summary, among the proposed solutions, the more-performing is **m-biGRU-max** that is realised by a bidirectional RNN with GRU and max pooling aggregation. However, from our numerical simulations, we have observed that the value of the total dynamical time, as well as M and Δ (see next paragraph), emerge to be crucial to correctly train the ML-models. Specifically, by taking a quantum dynamics with a short enough duration, also SVMs are able to classify quantum noise sources with very high accuracy. With short enough dynamics we mean short with respect to the time needed for the quantum walker in escaping from the initial node of the graph, which in our case is around $t_{15} = 0.1$ in natural units (n.u.). Instead, with t_{15} around 1 (in n.u.) only RNNs provide better results, and for $t_{15} \gg 1$, none of

the proposed ML-techniques solves quantum noise classification problems (these results have not been reported in Table III for the sake of simplicity). Moreover, it is also worth stressing that, if the duration of the noisy quantum dynamics is $t_{15} = 0.1$, ML-models efficiently classify quantum noise sources by only processing the last measured distribution $\mathcal{P}_{t_{15}}$. These findings can be relevant for effective implementation (also at the experimental level), since the training and tuning of SVM is orders of magnitude faster (e.g., around minutes vs hours or even days depending on the model) with respect to ANNs. The reason has to be found in the more complex structure of the ANNs than SVMs.

Furthermore, all our numerical results have shown that it is easier to classify between two different noisy quantum dynamics both affected by i.i.d. noise sources or by i.i.d. and coloured noise processes than between two noisy quantum dynamics subjected to coloured noise. Again it confirms the relevant role played by time-correlations and how the latter highly influence the value of the classification accuracy. Secondly, we expect that the same ML-techniques that we have exploited in this work could be successfully applied to classify among coloured quantum noise with q -step transition matrices $T_{t|t-q}$ with $q > 1$.

As final remark, let us observe that for simplicity we have assumed that the time instants when \mathcal{P}_{t_k} are measured are the same when \mathbf{g} is stochastically modified. This choice is dictated by the need to reduce the number of free parameters of the implemented classification task. Different configurations, with another choice of the noise changing rate, could be tested by applying our techniques to already existing quantum devices for quantum technology purposes.

Scaling of the classification accuracy

Let us now investigate the scaling of the classification accuracy γ as a function of Δ and M . Notice that Δ and M are related to the total dynamical time t_M , since $t_M \equiv M\Delta$ by taking Δ constant.

A possible explanation of the difference observed between the three previously-analysed scenarios, i.e., $t_{15} = 0.1$, $t_{15} = 1$ and $t_{15} \gg 1$ could be that the information on both the noise source and the initial quantum state – carried by the measured probability distributions \mathcal{P}_{t_k} – is lost during the system evolution, especially as the time increases. For such aspect, not only the total dynamical time could play a role, but also the time interval $\Delta \equiv t_1 - t_0 \equiv \dots \equiv t_M - t_{M-1}$. In fact, it is reasonable to conjecture that a ML-model, able to correctly classify our noisy quantum dynamics with $t_{15} = 1$ (thus, $M = 15$), can also work if $t_{M'} \gg 1$ but with $M' > 15$ and $\Delta' = \Delta$ where $\Delta' \equiv t_1 - t_0 \equiv \dots \equiv t_{M'} - t_{M'-1}$. In this way, the sequence $\mathcal{P}_{t_1}, \dots, \mathcal{P}_{t_{15}}$ is contained in $\mathcal{P}_{t_1}, \dots, \mathcal{P}_{t_{M'}}$. In other terms, we conjecture that the classification problem can be even solved for longer noisy quantum dynamics, but provided that Δ remains small.

To gain evidence on this conjecture, we have performed two additional experiments. Starting from the task **IID** with $t_{15} = 1$ with **m-biGRU-max** as baseline (accuracy 91.8%), the same model (optimised in the same hyperparameters space) is trained on two new data sets. For both data sets $t_M = 2$, with M equal to 15 for the first data set and 30 for the second one. Thus, in the former $\Delta' > \Delta$ with Δ time interval of the original data set, while in the latter $\Delta' = \Delta$. The first experiment ($\Delta' > \Delta$) provides a classification accuracy of 81.1%, contrarily to the results from the second experiment ($\Delta' = \Delta$), where a better accuracy of 96.3% is achieved. Accordingly, we have thus observed that, by taking $\Delta' = \Delta$ and the same ML-model, the classification problem can be solved even with an higher accuracy, but at the price of a longer training time. Indeed, in this case, the length of each sample of the data set is twice the original one.

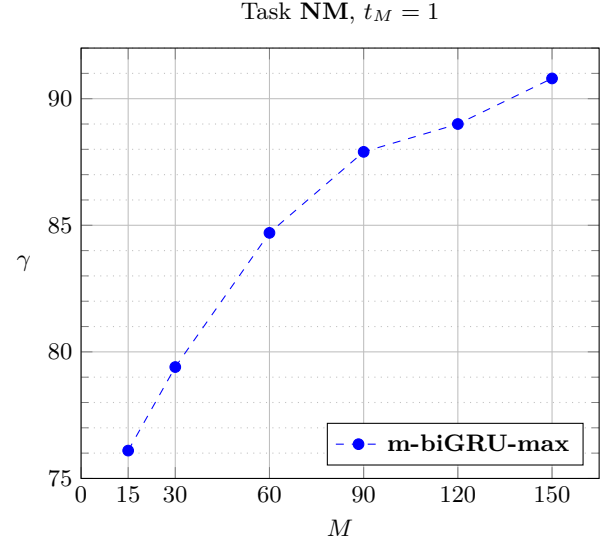


Figure 3. Percent classification accuracy γ vs. M . It refers to the test set associated to the model **m-biGRU-max** for the task **NM**. Specifically, the value of the total evolution time is fixed to $t_M = 1$. Notice that the first point of the figure corresponds to the value in Table III obtained for $t_{15} = 1$.

In another experiment, whose results are shown in Figure 3, we vary M by keeping the total evolution time equal to $t_M = 1$. Such tests use as baseline the model **m-biGRU-max** applied on the most difficult task of table III, i.e., **NM** with $t_{15} = 1$. As a result, the achieved classification accuracy is directly proportional to M and, thus, inversely proportional to the value of the time interval Δ . Indeed, by taking t_M fixed and reducing Δ , the classification accuracy of the same model can be enhanced. Specifically, it is possible to obtain more than 90% of accuracy also for the task **NM** with a total dynamical time equal to 1, at the price of a longer training time, since the length of the sequences increases.

Quantum advantages

Here, we address the following question: Could the proposed ML techniques be applied for the inference of noise sources affecting the dynamics of classical systems, e.g. Langevin equations [67]? Probably yes, but we expect that their application to quantum systems, maybe surprisingly, can be more effective than on classical systems. Both classical (non-periodic) dissipative dynamics [67] and stochastic quantum dynamics (stochastic due to the presence of an external environment, or noise sources as in our case) can asymptotically tend to a fixed-point, whereby the information on the initial state is lost. This means that the states of the system used for this noise classification tend to become indistinguishable as time increases. Classically, this can happen due to energy dissipation introduced by damping terms. Instead, quantum-mechanically, a dynamical fixed point can be reached due to decoherence that makes vanishing, at least on average, all quantum coherence terms [5]. Thus, once the transient of the evolution is elapsed, the evaluation of the final state of the system does not bring information neither on the initial state nor on the initial dynamics bringing the system to the asymptotic fixed-point. In our case, indeed, we have observed that, by using only $\mathcal{P}_{t_{15}}$ with long total dynamical time, the accuracy of all the classification tasks is always around 50% both for SVM and MLP. Consequently, if one aims to infer/reconstruct the value of parameters, signals or operators that influence the dynamics of the system by measuring its evolution, the most appropriate time window is during the transient. In this regard, a quantum dynamic, until it is nearly close of being unitary, is able to explore different configurations thanks to linearity and the quantum superposition principle. Conversely, classical dynamics, not being able to propagate superpositions of their trajectories, cannot provide per time unit the same amount of information on the quantity to be inferred.

In conclusion, the application of the proposed methods is expected to be more accurate if applied to quantum systems than classical ones, but during the transient of its dynamical evolution when quantum effects are still predominant and the distance among the state and the fixed point is not negligible. This conjecture will be properly discussed, and possibly numerically proved, in a forthcoming paper.

Outlooks

We plan to apply our techniques to characterize the noise in two different quantum devices as Q-IBM® and Rigetti® that, as other Noisy Intermediate-Scale Quantum prototypes [68], are unavoidably affected by external noise sources. In such experimental noise benchmarking, it could be convenient to fix the connections among single quantum gates (i.e., the underlying topology), and instead consider more realizations of the implemented

quantum dynamics affected by external noise. In this regard, we recall that, for the generation of the data set to train classification ML-models, having quantum gates with random connections could prevent that the models work accurately only for specific configurations. Moreover, the possibility to exploit reconfigurable experimental platforms [69, 70] could allow us to train our ML-models as proposed in this paper.

We also aim to use ML methods, and especially ANNs, to completely reconstruct quantum noise features. Our proposal is to derive accurate estimates of both the probability distribution $\text{Prob}(g)$ and the transition matrix T in case of time-correlated noise processes. Finally, we plan to extend our results to the classification of spatially-correlated noise sources, thus proposing very promising, and possibly more accurate, alternatives to other noise-sensing techniques recently discussed in Refs. [71, 72].

METHODS

Data set generation

In the data set generation, each sample of the data sets is created by first generating a random set of links \mathcal{E} (random topology) for the graph \mathcal{G} , and then initialising the quantum walker in a randomly chosen node of the graph. Hence, \mathcal{P}_{t_0} is a Kronecker delta centered in one of the 40 nodes. Then, we evolve the stochastic quantum dynamics for 15 steps, for each simulated noise source of the generated data set. All the probability distributions \mathcal{P}_{t_k} for $k = 0, \dots, 15$ are stored together with the attached label that indicates the associated type of noise.

Implementation of machine learning algorithms

All the ML-models are realized in *PyTorch* and have been trained on the six different data sets using a DELL® Precision Tower workstation with one NVIDIA® TITAN RTX® GPU with 10 Gb of memory, 88 cores Intel® Xeon® CPU E5-2699 v4 at 2.20GHz and 94 Gb of RAM.

We train the ANN models in mini-batches of dimension 16 by means of the SGD using ADAM [50] and learning rate $\eta = 10^{-3}$. We optimize the hyperparameters ξ with *ASHA* [73] as scheduler and *Hyperopt* [74, 75] (*Hyperopt* belongs to the family of Bayesian optimization algorithms) as search algorithm in the framework *Ray Tune* [76]. For the MLP models, the hyperparameter optimization defines: (i) the activation functions to be used, (ii) the number of layers, and (iii) their dimension, within the following search space: $\sigma \in \{\text{relu}, \text{sigmoid}, \text{tanh}\}$, $L \in \{2, 3, 4, 5, 6\}$ and $\dim(\mathbf{h}[1]) \equiv \dots \equiv \dim(\mathbf{h}[L]) \in \{d \in \mathbb{N} \mid 1 \leq d \leq 512\}$. Instead, for the RNN models the search space is $L \in \{1, 2, 3, 4\}$ for the number of recurrent layers ($L \in \{1, 2, 3, 4, 5, 6\}$ for the **NM** task with $t_{15} = 0.1$), and $\dim(\mathbf{h}_t[1]) \equiv \dim(\mathbf{h}_t[1]) \equiv \dots \equiv$

$\dim(\tilde{\mathbf{h}}_t[L]) \equiv \dim(\tilde{\mathbf{h}}_t[L]) \in \{d \in \mathbb{N} \mid 1 \leq d \leq 512\}$ for the layers dimension. Regarding the ML-models **m-biGRU-att** and **m-biLSTM-att**, the search space includes also the dimension of the attention layer as in Eqs. (20) and (21), i.e., $\dim(\mathbf{c}) \equiv \dim(\mathbf{v}_1) \equiv \dots \equiv \dim(\mathbf{v}_\tau) \in \{d \in \mathbb{N} \mid 1 \leq d \leq 512\}$. In the hyperparameter optimization of all the MLP and the RNN models, we have also used regularization methods as *weight decay* [77] and *dropout* [78]. They are able to mitigate overfitting; in particular, the former adds a penalty (chosen among $\{0, 10^{-4}, 10^{-3}\}$) to the risk function $L_S(\theta, \xi)$ with the aim to discourage large weights. Instead, using dropout, the outputs of the single artificial neurons during the training are forced to zero with a probability among $\{0, 0.2, 0.5\}$.

ACKNOWLEDGMENTS

The authors were financially supported from by the Fondazione CR Firenze through the project QUANTUM-AI, the European Union’s Horizon 2020 research and innovation programme under FET-OPEN Grant Agreement No. 828946 (PATHOS), and from University of Florence through the project Q-CODYCES.

DATA AND CODE AVAILABILITY

The source codes for the generation of the data sets and the ML experiments are available on *GitHub* at the following address:

<https://github.com/trianam/quantumNoiseClassification>.

[1] Jared H Cole and Lloyd CL Hollenberg. Scanning quantum decoherence microscopy. *Nanotechnology*, 20(49):495401, 2009.

[2] Jonas Bylander, Simon Gustavsson, Fei Yan, Fumiki Yoshihara, Khalil Harrabi, George Fitch, David G Cory, Yasunobu Nakamura, Jaw-Shen Tsai, and William D Oliver. Noise spectroscopy through dynamical decoupling with a superconducting flux qubit. *Nature Physics*, 7(7):565–570, 2011.

[3] Christian L Degen, F Reinhard, and Paola Cappellaro. Quantum sensing. *Reviews of modern physics*, 89(3):035002, 2017.

[4] Piotr Szałkowski, Guy Ramon, Jan Krzywda, Damian Kwiatkowski, et al. Environmental noise spectroscopy with qubits subjected to dynamical decoupling. *Journal of Physics: Condensed Matter*, 29(33):333001, 2017.

[5] Heinz-Peter Breuer and Francesco Petruccione. *The theory of open quantum systems*. Oxford University Press on Demand, 2002.

[6] Filippo Caruso, Vittorio Giovannetti, Cosmo Lupo, and Stefano Mancini. Quantum channels and memory effects. *Reviews of Modern Physics*, 86(4):1203, 2014.

[7] Matthias M Müller, Stefano Gherardini, and Filippo Caruso. Stochastic quantum Zeno-based detection of noise correlations. *Scientific reports*, 6:38650, 2016.

[8] Stefano Gherardini. *Noise as a resource*. PhD thesis, University of Florence, Italy, 2018. arXiv preprint arXiv:1805.01800.

[9] Gerardo A Paz-Silva and Lorenza Viola. General transfer-function approach to noise filtering in open-loop quantum control. *Physical review letters*, 113(25):250501, 2014.

[10] Leigh M Norris, Gerardo A Paz-Silva, and Lorenza Viola. Qubit noise spectroscopy for non-Gaussian dephasing environments. *Physical Review Letters*, 116(15):150503, 2016.

[11] V.M. Frey, S. Mavadia, L.M. Norris, W. de Ferranti, D. Lucarelli, Viola L., and M.J. Biercuk. Application of optimal band-limited control protocols to quantum noise sensing. *Nat. Commun.*, 8:2189, Dec 2017.

[12] Matthias M Müller, Stefano Gherardini, and Filippo Caruso. Noise-robust quantum sensing via optimal multi-probe spectroscopy. *Scientific Reports*, 8(1):1–17, 2018.

[13] Santiago Hernández-Gómez, Francesco Poggiali, Paola Cappellaro, and Nicole Fabbri. Noise spectroscopy of a quantum-classical environment with a diamond qubit. *Physical Review B*, 98(21):214307, 2018.

[14] Youngkyu Sung, Félix Beaudoin, Leigh M Norris, Fei Yan, David K Kim, Jack Y Qiu, Uwe von Lüpke, Joni-lyn L Yoder, Terry P Orlando, Simon Gustavsson, et al. Non-Gaussian noise spectroscopy with a superconducting qubit sensor. *Nature communications*, 10(1):1–8, 2019.

[15] Hoang-Van Do, Cosimo Lovecchio, Ivana Mastroserio, Nicole Fabbri, Francesco S Cataliotti, Stefano Gherardini, Matthias M Müller, Nicola Dalla Pozza, and Filippo Caruso. Experimental proof of quantum Zeno-assisted noise sensing. *New Journal of Physics*, 21(11):113056, 2019.

[16] Jan Krzywda, Piotr Szałkowski, and Łukasz Cywiński. The dynamical-decoupling-based spatiotemporal noise spectroscopy. *New Journal of Physics*, 21(4):043034, 2019.

[17] Matthias M Müller, Stefano Gherardini, Nicola Dalla Pozza, and Filippo Caruso. Noise sensing via stochastic quantum Zeno. *Physics Letters A*, 384(13):126244, 2020.

[18] Akram Youssry, Gerardo A Paz-Silva, and Christopher Ferrie. Beyond Quantum Noise Spectroscopy: modelling and mitigating noise with quantum feature engineering. *npj Quantum Information*, 6:95, 2020.

[19] Gonzalo A Álvarez and Dieter Suter. Measuring the spectrum of colored noise by dynamical decoupling. *Physical review letters*, 107(23):230501, 2011.

[20] Tatsuro Yuge, Susumu Sasaki, and Yoshiro Hirayama. Measurement of the noise spectrum using a multiple-pulse sequence. *Physical review letters*, 107(17):170504, 2011.

[21] F Poggiali, P Cappellaro, and N Fabbri. Optimal control for one-qubit quantum sensing. *Physical Review X*, 8(2):021059, 2018.

[22] Łukasz Cywiński. Dynamical-decoupling noise spectroscopy at an optimal working point of a qubit. *Physical Review A*, 90(4):042307, 2014.

[23] Nicola Dalla Pozza, Stefano Gherardini, Matthias M Müller, and Filippo Caruso. Role of the filter functions in noise spectroscopy. *International Journal of Quantum Information*, 17(08):1941008, 2019.

[24] Robin Harper, Steven T Flammia, and Joel J Wallman. Efficient learning of quantum noise. *Nature Physics*, pages 1–5, 2020.

[25] Shai Shalev-Shwartz and Shai Ben-David. *Understanding machine learning: From theory to algorithms*. Cambridge university press, 2014.

[26] Trevor Hastie, Robert Tibshirani, and Jerome Friedman. *The elements of statistical learning: data mining, inference, and prediction*. Springer Science & Business Media, 2009.

[27] Angel Rivas, Susana F Huelga, and Martin B Plenio. Quantum non-Markovianity: characterization, quantification and detection. *Reports on Progress in Physics*, 77(9):094001, 2014.

[28] Heinz-Peter Breuer, Elsi-Mari Laine, Jyrki Piilo, and Bassano Vacchini. Colloquium: Non-Markovian dynamics in open quantum systems. *Reviews of Modern Physics*, 88(2):021002, 2016.

[29] Yakir Aharonov, Luiz Davidovich, and Nicim Zagury. Quantum random walks. *Physical Review A*, 48(2):1687, 1993.

[30] Julia Kempe. Quantum random walks: an introductory overview. *Contemporary Physics*, 44(4):307–327, 2003.

[31] Viv Kendon. Decoherence in quantum walks—a review. *Mathematical structures in computer science*, 17(6):1169–1220, 2007.

[32] Salvador Elías Venegas-Andraca. Quantum walks: a comprehensive review. *Quantum Information Processing*, 11(5):1015–1106, 2012.

[33] Nicola Dalla Pozza and Filippo Caruso. Quantum state discrimination on reconfigurable noise-robust quantum networks. *Physical Review Research*, 2(4):043011, 2020.

[34] Christopher M Bishop. *Pattern recognition and machine learning*. Springer, 2006.

[35] Ian Goodfellow, Yoshua Bengio, and Aaron Courville. *Deep learning*. MIT press Cambridge, 2016. <http://www.deeplearningbook.org>.

[36] Jürgen Schmidhuber. Deep learning in neural networks: An overview. *Neural networks*, 61:85–117, 2015.

[37] Yoav Goldberg. Neural network methods for natural language processing. *Synthesis Lectures on Human Language Technologies*, 10(1):1–309, 2017.

[38] Wolfgang Paul and Jörg Baschnagel. *Stochastic processes*, volume 1. Springer, 2013.

[39] Olga Russakovsky, Jia Deng, Hao Su, Jonathan Krause, Sanjeev Satheesh, Sean Ma, Zhiheng Huang, Andrej Karpathy, Aditya Khosla, Michael Bernstein, et al. Imagenet large scale visual recognition challenge. *International journal of computer vision*, 115(3):211–252, 2015.

[40] Alex Krizhevsky, Ilya Sutskever, and Geoffrey E Hinton. Imagenet classification with deep convolutional neural networks. *Communications of the ACM*, 60(6):84–90, 2017.

[41] F Emmert-Streib, Z Yang, H Feng, S Tripathi, and M Dehmer. An introductory review of deep learning for prediction models with big data. *Artif. Intell.*, 3(4), 2020.

[42] Xavier Glorot, Antoine Bordes, and Yoshua Bengio. Deep sparse rectifier neural networks. In *Proceedings of the fourteenth international conference on artificial intelligence and statistics*, pages 315–323, 2011.

[43] Vinod Nair and Geoffrey E Hinton. Rectified linear units improve restricted Boltzmann machines. In *ICML*, 2010.

[44] Kurt Hornik, Maxwell Stinchcombe, Halbert White, et al. Multilayer feedforward networks are universal approximators. *Neural networks*, 2(5):359–366, 1989.

[45] Rich Caruana, Steve Lawrence, and C Lee Giles. Overfitting in neural nets: Backpropagation, conjugate gradient, and early stopping. In *Advances in neural information processing systems*, pages 402–408, 2001.

[46] James Bergstra and Yoshua Bengio. Random search for hyper-parameter optimization. *The Journal of Machine Learning Research*, 13(1):281–305, 2012.

[47] Jasper Snoek, Hugo Larochelle, and Ryan P Adams. Practical Bayesian optimization of machine learning algorithms. *Advances in neural information processing systems*, 25:2951–2959, 2012.

[48] Léon Bottou. Large-scale machine learning with stochastic gradient descent. In *Proceedings of COMPSTAT’2010*, pages 177–186. Springer, 2010.

[49] Tong Zhang. Solving large scale linear prediction problems using stochastic gradient descent algorithms. In *Proceedings of the twenty-first international conference on Machine learning*, page 116, 2004.

[50] Diederik P Kingma and Jimmy Ba. Adam: A method for stochastic optimization. *arXiv preprint arXiv:1412.6980*, 2014.

[51] Stefano Martina, Leonardo Ventura, and Paolo Frasconi. Classification of cancer pathology reports: a large-scale comparative study. *IEEE Journal of Biomedical and Health Informatics*, 24(11):3085–3094, 2020.

[52] Stefano Martina. *Classification of cancer pathology reports with Deep Learning methods*. PhD thesis, University of Florence, Italy, 3 2020.

[53] Duyu Tang, Bing Qin, and Ting Liu. Document modeling with gated recurrent neural network for sentiment classification. In *Proceedings of the 2015 conference on empirical methods in natural language processing*, pages 1422–1432, 2015.

[54] Herbert Jaeger and Harald Haas. Harnessing nonlinearity: Predicting chaotic systems and saving energy in wireless communication. *science*, 304(5667):78–80, 2004.

[55] Zachary C Lipton, John Berkowitz, and Charles Elkan. A critical review of recurrent neural networks for sequence learning. *arXiv preprint arXiv:1506.00019*, 2015.

[56] Ilya Sutskever, Oriol Vinyals, and Quoc V Le. Sequence to sequence learning with neural networks. In *Advances in neural information processing systems*, pages 3104–3112, 2014.

[57] Sepp Hochreiter. The vanishing gradient problem during learning recurrent neural nets and problem solutions. *International Journal of Uncertainty, Fuzziness and Knowledge-Based Systems*, 6(02):107–116, 1998.

[58] Yoshua Bengio, Patrice Simard, and Paolo Frasconi. Learning long-term dependencies with gradient descent is difficult. *IEEE transactions on neural networks*, 5(2):157–166, 1994.

[59] Sepp Hochreiter and Jürgen Schmidhuber. Long short-term memory. *Neural computation*, 9(8):1735–1780, 1997.

[60] Kyunghyun Cho, Bart van Merriënboer, Caglar Gulcehre, Dzmitry Bahdanau, Fethi Bougares, Holger Schwenk, and Yoshua Bengio. Learning phrase representations using RNN encoder-decoder for statistical machine translation. In *Proceedings of the 2014 Conference*

on Empirical Methods in Natural Language Processing (EMNLP), pages 1724–1734, 2014.

[61] Dzmitry Bahdanau, Kyunghyun Cho, and Yoshua Bengio. Neural machine translation by jointly learning to align and translate. In *3rd International Conference on Learning Representations, ICLR 2015*, 2015.

[62] Minh-Thang Luong, Hieu Pham, and Christopher D Manning. Effective approaches to attention-based neural machine translation. *arXiv preprint arXiv:1508.04025*, 2015.

[63] Jan K Chorowski, Dzmitry Bahdanau, Dmitriy Serdyuk, Kyunghyun Cho, and Yoshua Bengio. Attention-based models for speech recognition. *Advances in neural information processing systems*, 28:577–585, 2015.

[64] Zichao Yang, Diyi Yang, Chris Dyer, Xiaodong He, Alex Smola, and Eduard Hovy. Hierarchical attention networks for document classification. In *Proceedings of the 2016 conference of the North American chapter of the association for computational linguistics: human language technologies*, pages 1480–1489, 2016.

[65] Alex Graves. Sequence transduction with recurrent neural networks. *arXiv preprint arXiv:1211.3711*, 2012.

[66] Yann LeCun, Yoshua Bengio, and Geoffrey Hinton. Deep learning. *nature*, 521(7553):436–444, 2015.

[67] S.R. De Groot and P. Mazur. *Non-Equilibrium Thermodynamics*. Dover Publications, 1984.

[68] John Preskill. Quantum Computing in the NISQ era and beyond. *Quantum*, 2:79, 2018.

[69] Johannes Nokkala, Francesco Arzani, Fernando Galve, Roberta Zambrini, Sabrina Maniscalco, Jyrki Piilo, Nicolas Treps, and Valentina Parigi. Reconfigurable optical implementation of quantum complex networks. *New Journal of Physics*, 20(5):053024, 2018.

[70] Saroch Leedumrongwatthanakun, Luca Innocenti, Hugo Defienne, Thomas Juffmann, Alessandro Ferraro, Mauro Paternostro, and Sylvain Gigan. Programmable linear quantum networks with a multimode fibre. *Nature Photonics*, 14(3):139–142, 2020.

[71] Gerardo A Paz-Silva, Leigh M Norris, Félix Beaudoin, and Lorenza Viola. Extending comb-based spectral estimation to multiaxis quantum noise. *Physical Review A*, 100(4):042334, 2019.

[72] Virginia Frey, Leigh M. Norris, Lorenza Viola, and Michael J. Biercuk. Simultaneous Spectral Estimation of Dephasing and Amplitude Noise on a Qubit sensor via Optimally Band-Limited Control. *Phys. Rev. Applied*, 14:024021, Aug 2020.

[73] Liam Li, Kevin Jamieson, Afshin Rostamizadeh, Ekaterina Gonina, Jonathan Ben-Tzur, Moritz Hardt, Benjamin Recht, and Ameet Talwalkar. A system for massively parallel hyperparameter tuning. *Proceedings of Machine Learning and Systems*, 2:230–246, 2020.

[74] James S Bergstra, Rémi Bardenet, Yoshua Bengio, and Balázs Kégl. Algorithms for hyper-parameter optimization. In *Advances in neural information processing systems*, pages 2546–2554, 2011.

[75] James Bergstra, Daniel Yamins, and David Cox. Making a science of model search: Hyperparameter optimization in hundreds of dimensions for vision architectures. In *International conference on machine learning*, pages 115–123. PMLR, 2013.

[76] Richard Liaw, Eric Liang, Robert Nishihara, Philipp Moritz, Joseph E Gonzalez, and Ion Stoica. Tune: A research platform for distributed model selection and training. *arXiv preprint arXiv:1807.05118*, 2018.

[77] Anders Krogh and John A Hertz. A simple weight decay can improve generalization. In *Advances in neural information processing systems*, pages 950–957, 1992.

[78] Nitish Srivastava, Geoffrey Hinton, Alex Krizhevsky, Ilya Sutskever, and Ruslan Salakhutdinov. Dropout: a simple way to prevent neural networks from overfitting. *The journal of machine learning research*, 15(1):1929–1958, 2014.